Strong Support for the Millisecond Pulsar Origin of the Galactic Center GeV Excess

Bartels, R.; Krishnamurthy, S.; Weniger, C.

DOI
10.1103/PhysRevLett.116.051102

Publication date
2016

Document Version
Other version

Published in
Physical Review Letters

Strong Support for the Millisecond Pulsar Origin of the Galactic Center GeV Excess: Supplementary Material

Richard Bartels,[1,*] Suraj Krishnamurthy,[1,†] and Christoph Weniger[1,‡]

[1] *GRAPPA Institute, University of Amsterdam, Science Park 904, 1090 GL Amsterdam, Netherlands*

(Dated: December 12, 2015)

In the supplementary material, we discuss the possible impact of various systematic effects on our results. This includes a control region analysis, a discussion of various types of γ-ray sources, substructure in diffuse emission, a thick-disk population of MSPs, sphericity and the role of negative wavelet peaks.

A. Null results in control regions

In order to estimate the effect of various systematic uncertainties, it is useful to apply our analysis on control regions along the Galactic disk (in the case of Galactic diffuse emission this was first systematically done in Ref. [1]). Potentially unresolved substructure in the Galactic diffuse emission (e.g. in the form of giant molecular clouds, see below), and contributions from various Galactic and extragalactic source populations could be responsible for the detected wavelet signal in the inner Galaxy, but would in general also affect other regions in the Galactic disk. To this end, we focus on (partially overlapping) control regions along the Galactic disk, which are of the same size as the inner Galaxy ROI, but displaced by $\Delta\ell = \pm k\, 20^\circ$ with $k = 1, 2, 3, 4$.

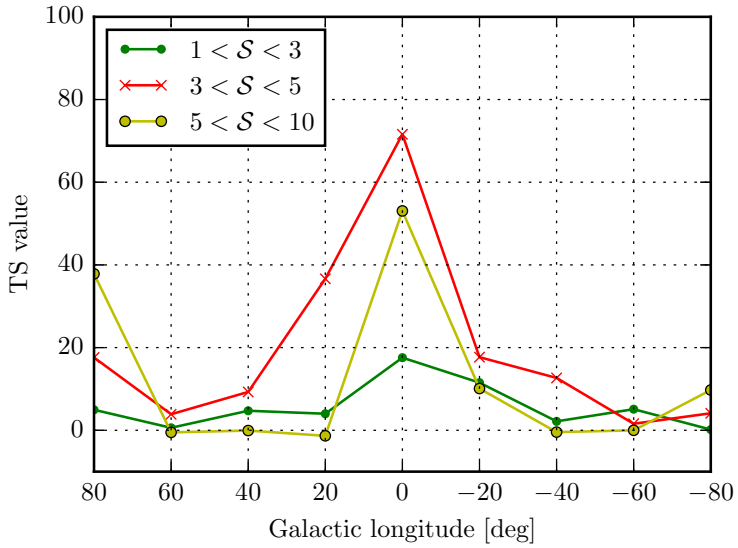

FIG. S-1. We show, as function of the central longitudinal position of the control regions (for $\ell = 0^\circ$ the main ROI), the significance of a CSP detection. We assume that the CSP is centered in each of the ROIs, and we refit the parameters $L_{\rm max}$ and the number of sources. We indicate how different ranges of the wavelet peak significances contribute to the detection. *All* 3FGL sources are masked in this plot, in order to be conservative.

In Fig. S-1 we show the TS value for a detection of the CSP for the main and the different control ROIs along the Galactic disk. We leave $L_{\rm max}$ and Φ_5 free to vary in each region independently. In the main ROI that covers the inner Galaxy we find the significant detection of a CSP that was discussed in the main text. As shown in the plot, this high significance is supported by the low, intermediate and high-significance SNR peaks of the wavelet transform separately. The directly adjacent regions also show relatively large TS values, which is either caused by the partial overlap of these control regions with the main ROI, or by a CSP that is more disk-like than assumed in our analysis. We will address the latter point below. However, in the outermost six control regions we find no significant detection of a CSP, for any of the considered values for $L_{\rm max}$ and Φ_5 (the large TS values at $\ell = 80^\circ$ are caused by one extremely bright source that generates fake peaks in its tails). This observation makes it already extremely unlikely that our

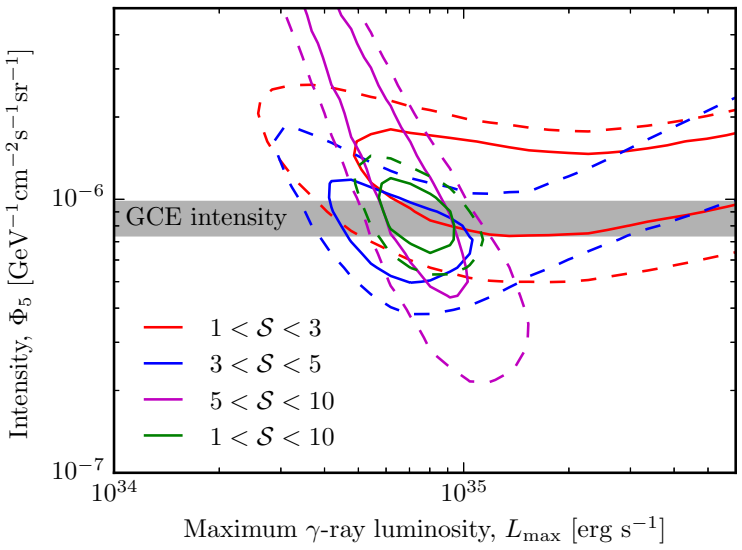

FIG. S-2. Similar to Fig. 3 in the main text, but showing limits derived for different ranges of the wavelet peak significances separately. The parameter degeneracies present in some of the fits cancel when fitting the entire significance range at once. We only show 68.7% and 95.4% CL constraints for clarity.

findings are driven by a mismodelling of the local Galactic diffuse emission, or by extragalactic sources. We will address this in more detail below.

B. Consistent wavelet signal in separate bins

It is instructive to see how wavelet peaks with different significances contribute to the constraints on the luminosity function that we showed in Fig. 3 in the main text. To this end, we show in Fig. S-2 the limits that we obtain separately from peak significances in the range $\mathcal{S} = 1$–3, $\mathcal{S} = 3$–5 and $\mathcal{S} = 5$–10, respectively. All three constraints are mutually consistent to within 1σ, leading to a consistent interpretation of the peaks shown in Fig. 1 in the main text. In all cases we find some degeneracy in the ($L_{\rm max}$, Φ_5) plane. High significance peaks predominantly provide a stringent upper limit on $L_{\rm max}$, whereas low significance peaks mostly constrain the overall luminosity of the modelled source population.

To show that our assumption on the spatial distribution of the CSP is consistent with the data, we show Fig. S-3 the result obtained for the five different spatial bins independently. Ring 1–5 correspond to $r \in [i^\circ, i + 3^\circ]$ with $i = 2, 5, 8, 11, 14$, respectively. We find constraints on $L_{\rm max}$ and Φ_5 that are mostly consistent to within 1σ.

Finally, we checked that the identified wavelet peaks are symmetrically distributed in the north, south, east and west parts of our main ROI. Only at $S > 3$ we find a slight (statistically not very significant) asymmetry with more peaks in the south, which might be caused by the somewhat stronger Galactic foregrounds in the north, which makes point source detection in the north more challenging.

C. Mild dependence on the MSP luminosity function

Theoretically, α is not well constrained and can plausibly range from 1.5 to 3, depending on the emission model [2–4]. Actual MSP observations actually seem to indicate somewhat smaller values closer to $\alpha \sim 1.2$ [5]. We show in Fig. S-4 the 68.7% and 95.4% CL contours for different luminosity functions, respectively with spectral indices of 1.2 and 1.7. For a fixed intensity (Φ_5), hardening (softening) of the luminosity function corresponds to an enhancement (suppression) of the number of sub-threshold point sources, which explains the direction in which the best fit region moves. We note that we obtain very similar TS values for all slopes that we considered.

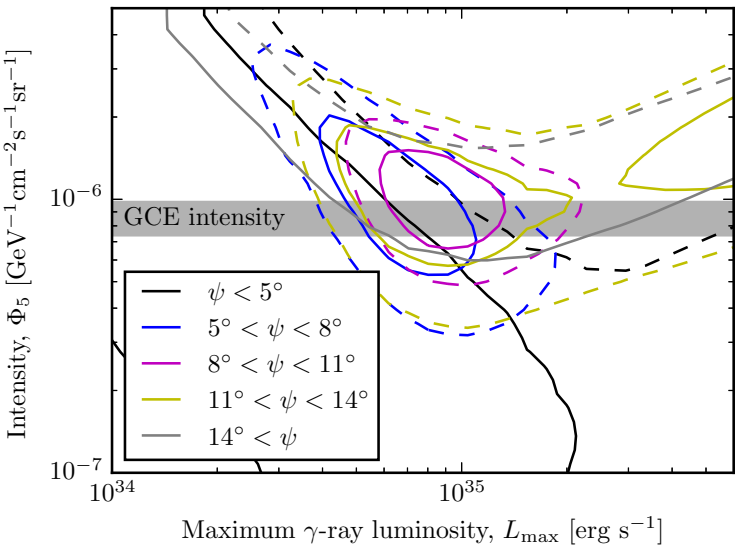

FIG. S-3. Similar to Fig. 3 in the main text, but showing limits as derived for different spatial bins separately.

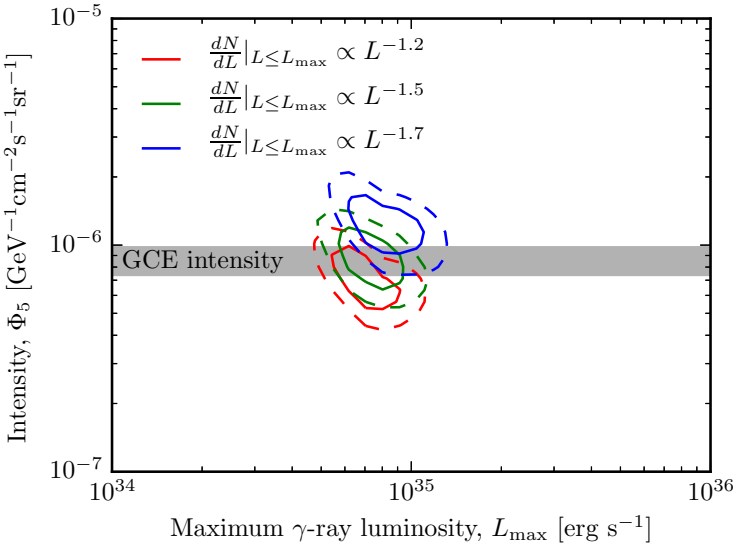

FIG. S-4. Similar to Fig. 3 in the main text. We show the 68.7% and 95.4% CL contours for luminosity functions with spectral indices of 1.2, 1.5 and 1.7.

D. The role of unmasked 3FGL sources

In the present analysis, we make use of the 3FGL, the third *Fermi* source catalogue, which is based on the first four years of *Fermi* pass 7 data. One important ingredient in our analysis is the masking of 3FGL sources. These sources are of Galactic and extragalactic origin and leaving them unmasked would inevitably induce sizeable signals in our search for a sub-threshold source population in the bulge. However, as discussed in the main text, we keep unassociated sources with MSP-like spectra unmasked. These sources could be part of the bulge MSP population that we are looking for, and masking them would bias our results. The 13 sources that pass our MSP cuts are listed in Tab. I.

In general, falsely masking unassociated sources that actually belong to the bulge MSP population would push $L_{\rm max}$ to lower values, whereas falsely unmasking foreground sources would push it to large values. This is illustrated

3FGL Name	$\ell\,[^\circ]$	$b\,[^\circ]$	χ^2/dof	$\sqrt{TS}$	$\mathcal{S}$	$L\,[10^{34}\,\mathrm{erg/s}]$
J1649.6-3007	-7.99	9.27	1.07	5.6	7.4	$7.8^{+5.5}_{-2.7}$
J1703.6-2850	-5.08	7.65	0.48	2.4	5.0	$3.4^{+2.4}_{-1.2}$
J1740.5-2642	1.30	2.12	0.37	6.4	3.5	$14.9^{+10.6}_{-5.1}$
J1740.8-1933	7.43	5.83	0.77	1.9	2.3	$3.8^{+2.7}_{-1.3}$
J1744.8-1557	11.03	6.88	0.40	3.7	3.4	$5.6^{+3.9}_{-1.9}$
J1758.8-4108	-9.21	-8.48	0.90	5.6	3.8	$4.8^{+3.4}_{-1.7}$
J1759.2-3848	-7.11	-7.43	0.35	4.6	5.6	$5.9^{+4.2}_{-2.0}$
J1808.3-3357	-1.94	-6.71	0.40	6.9	6.3	$8.0^{+5.7}_{-2.7}$
J1808.4-3519	-3.15	-7.36	0.41	4.6	4.4	$5.0^{+3.5}_{-1.7}$
J1808.4-3703	-4.68	-8.19	0.22	4.9	5.3	$4.3^{+3.1}_{-1.5}$
J1820.4-3217	0.74	-8.17	1.04	5.7	1.7	$7.2^{+5.1}_{-2.5}$
J1830.8-3136	2.35	-9.84	0.54	5.9	6.0	$5.0^{+3.6}_{-1.7}$
J1837.3-2403	9.85	-7.81	0.28	4.0	3.0	$4.7^{+3.3}_{-1.6}$

TABLE I. List of the 13 unassociated 3FGL sources with MSP-like spectra, which we leave unmasked in our analysis. If the GeV excess is caused by dim point sources, it is likely that some or most of them are part of the CSP. The last four columns show the goodness-of-fit of the reference MSP spectrum, the 3FGL significance in the 1–3 GeV band, the corresponding peak of the wavelet SNR, and the γ-ray luminosity (assuming 8.5 ± 2 kpc distance from the source and the reference stacked MSP spectrum from the main paper with a normalization that is obtained from a fit to the measured source flux).

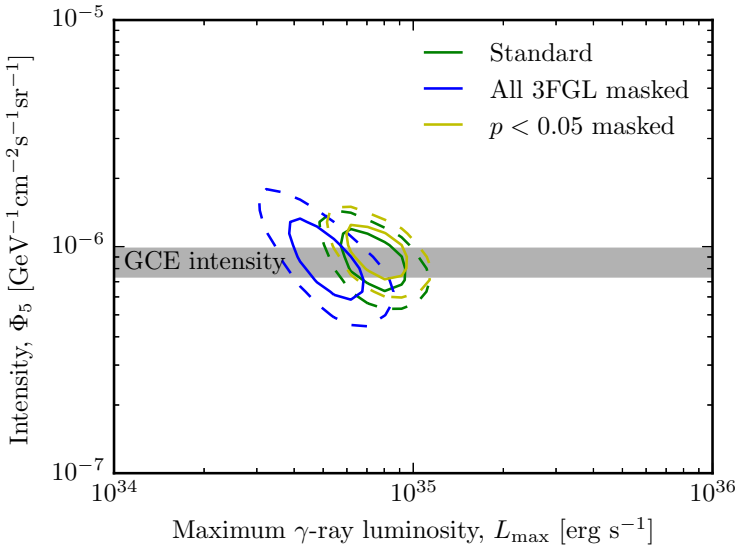

FIG. S-5. Similar to Fig. 3 in the main text. We show the effect of masking *all* 3FGL sources, or leaving a slightly larger number unmasked.

in Fig. S-5. We show the case where we mask *all* unassociated sources, as well as the case where we adopt a weaker criterion for the spectral fit, leaving around 20 sources unmasked. We find that in both cases the best-fit value for $L_{\rm max}$ moves in the expected direction, but the results remain consistent to within 1σ. Furthermore, the significance of our wavelet detection that we quote in the main text (where we include $\mathcal{S} < 5$ bins only) changes to 9.2σ when we mask all sources, and to 10.8σ when keeping 20 sources unmasked. The (un-)masking of 3FGL is hence not decisive for our qualitative findings, although quantitative results can be affected.

It is interesting to note that the faintest 3FGL source in the inner Galaxy ROI that passes our MSP-spectrum cut, has a luminosity of $L = 3.4 \times 10^{34}\,\mathrm{erg\,s^{-1}}$ if placed at 8.5 kpc distance. This is a good, though rough, indication for the *de facto* sensitivity threshold of *Fermi*-LAT for the detection of sources with MSP-like spectra in the bulge region.

Lastly, one can use the sources in Tab. I to compare the sensitivity of the 3FGL with our wavelet analysis. Averaging over the 13 sources, we find a ratio of $\mathcal{S}/\sqrt{TS} \simeq 1.0 \pm 0.4$, indicating that the sensitivity of the wavelet method is

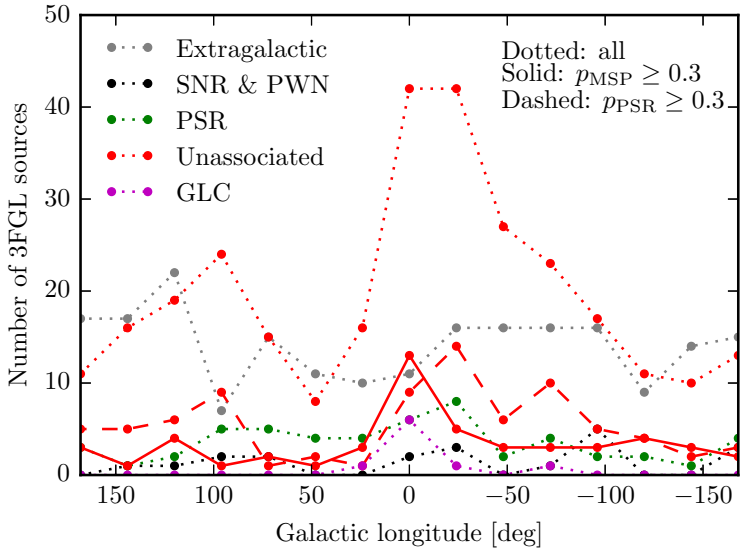

FIG. S-6. Latitude profile of sources, for different ROIs along the Galactic disk, as function of their longitudinal center (dotted lines). The ROIs have a size of $24^\circ \times 24^\circ$, with the Galactic disk, $|b| < 2^\circ$, masked. The different colors correspond to different source categories. In the case of unassociated sources, the solid (dashed) lines show only sources that pass the spectrum cut for MSP-like (young pulsar-like) sources.

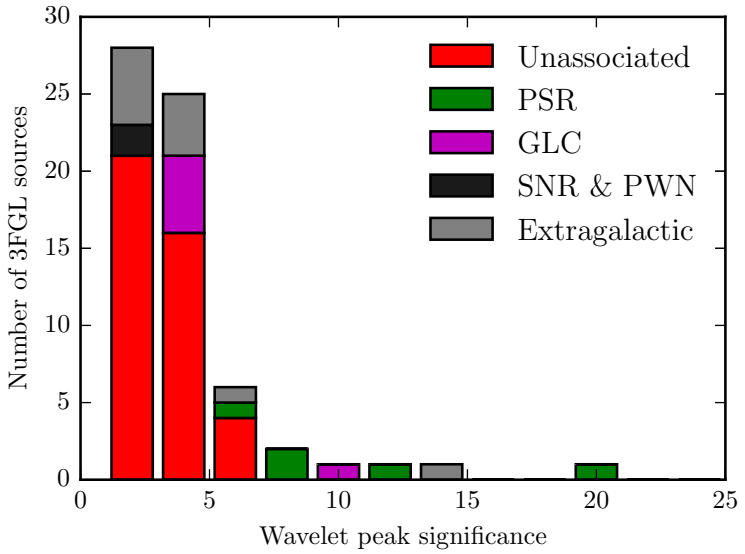

FIG. S-7. Stacked histogram of wavelet peak values $\mathcal{S}$ that correspond to 3FGL sources in the inner Galaxy ROI. We show the contribution from different source categories separately. Unassociated sources generate mostly low-significance wavelet peaks, whereas for example source that are marked as pulsar in the 3FGL only generate peaks with a high significance (see discussion).

similar to the 3FGL sensitivity in a comparable energy range. However, the scatter exceeds the one expected from statistical fluctuations alone, which can be attributed to differences in the systematics that affect the 3FGL and the wavelet analysis.

E. The role of various source populations

In Fig. S-6, we show the number of 3FGL sources in our inner Galaxy ROI as well as in various same-sized ROIs that are displaced along the Galactic disk in steps of $\Delta\ell = \pm 24^\circ$. We show (identified and associated) extragalactic sources, various Galactic source classes and unassociated sources classes separately. We also show for the unassociated sourced how many sources pass our MSP cut. It is apparent that the number of unassociated sources strongly peaks in the inner Galaxy ROI, however with a clear asymmetry towards negative values of ℓ, and another peak around $\ell \approx 100^\circ$. However, after applying the MSP cut, predominantly sources in the inner Galaxy survive. In Fig. S-7, on the other hand, we show a histogram of the wavelet peak significance that our analysis attributes to the 3FGL sources in the inner Galaxy ROI. Again, unassociated sources play a major role and produce wavelet peaks down to values of $\mathcal{S} \sim 1$. On the other hand, 3FGL sources that are identified as pulsars appear only with $\mathcal{S} > 5$ in our analysis. We will discuss in the following the potential impact of each of the source classes separately.

Extragalactic sources. As shown in Fig. S-6, the number of extragalactic sources in the individual ROIs along the Galactic disk fluctuates around values of about ~ 13. No significant suppression is observed in the inner Galaxy ROI, which would have indicated that it is more challenging to identify or associate extragalactic sources in this region. We will use here a simple argument to show that extragalactic sources cannot play a significant role for our results. The average number of $\mathcal{S} = 3$–5 wavelet peaks in the above control regions along the Galactic disk is 20; in the inner Galaxy ROI it is 42 (we exclude here *all* 3FGL sources to be conservative). If extragalactic sources were the main contribution to these peaks, in addition to the about 10 wavelet peaks that are expected from statistical fluctuations alone (see Fig. 2 in the main text), the 42 observed peaks would constitute a $> 5\sigma$ upward fluctuation above the expected 20. This makes it extremely unlikely that extragalactic sources contribute significantly to our results in the inner Galaxy. Similar arguments can be made using wavelet peaks in the range $\mathcal{S} = 1$–2.

Supernova remnants and pulsar wind nebulae. As apparent in Fig. S-6, only a very small number of sources along the Galactic disk at latitudes $|b| > 2^\circ$ (and almost none at $|b| > 5^\circ$) are identified with supernova remnants or pulsar wind nebulae. In our ROIs their number is much less than the number of extragalactic sources, and their distribution is centrally not peaked, indicating that sources at these latitudes are mostly local. Sources in this category are typically more easily detectable at higher and lower energies than the energy range used in our analysis, and would be most likely listed in the 3FGL and hence masked if they were abundant and significant. We consider it hence as extremely unlikely that sources of this category significantly affect our results in the inner Galaxy.

Young and millisecond pulsars. An interesting feature of pulsars in the 3FGL is that they always induce large wavelet signals in our analysis, as shown in Fig. S-7. This makes indeed sense, since the identification of a γ-ray source as pulsar requires the measurement of its pulsation, and hence a large enough number of photons. Furthermore, the pulsar energy spectrum often peaks close the energy range of our analysis. Already from Fig. S-7 it is obvious that a large fraction of the unassociated sources, which mostly appear with lower significance peaks, must in fact be pulsars. Interestingly, as shown in Fig. S-6, identified pulsars do not show a centrally peaked distribution, whereas the unassociated sources clearly do. This behaviour is expected, given that with increasing distance the pulsar identification becomes more challenging.

Globular clusters. The γ-ray emission from globular clusters that is not masked in our analysis, either because the globular clusters did not enter the 3FGL, or because they happen to be among our 13 unmasked unassociated sources, could in principle contribute to the detected signal. Since their total emission is usually due to several MSPs which appear as a single source for *Fermi*-LAT, their presence could bias $L_{\rm max}$ towards larger values. However, given the simulation results from Ref. [6], we expect this effect to be small, and leave a more detailed discussion to future work.

Unassociated sources. The peak of unassociated sources in the inner Galaxy, as shown in Fig. S-6, appears clearly asymmetric, with a second peak at $\ell \approx 100^\circ$. As discussed above, a large fraction of these sources is expected to be young or millisecond pulsars. Obviously, the 3FGL unassociated sources do not directly contribute to our results since they are masked (except the 13 MSP candidates). However, the unassociated sources are extremely abundant even down to $\mathcal{S} \sim 1$, and their probable nature can be used as an indicator for what source population dominates just below threshold.

In Fig. S-6, we see that our MSP cut removes most of the unassociated sources, but leaves an excess of 13 unassociated sources in the inner Galaxy, as discussed above. What is more, if we slightly modify the spectral criterion, using $dN/dE \propto e^{-E/2\,\mathrm{GeV}} E^{-2}$, which is somewhat more pulsar-like (softer index, lower cutoff), this behaviour changes and we instead find excesses that are more correlated with the peaks of the unassociated sources away from the inner Galaxy. Although the statistical significance of this finding is rather difficult to quantify without a detailed study (which we leave for future work), this result is indicative. It suggests that a large fraction of the inner Galaxy unas-

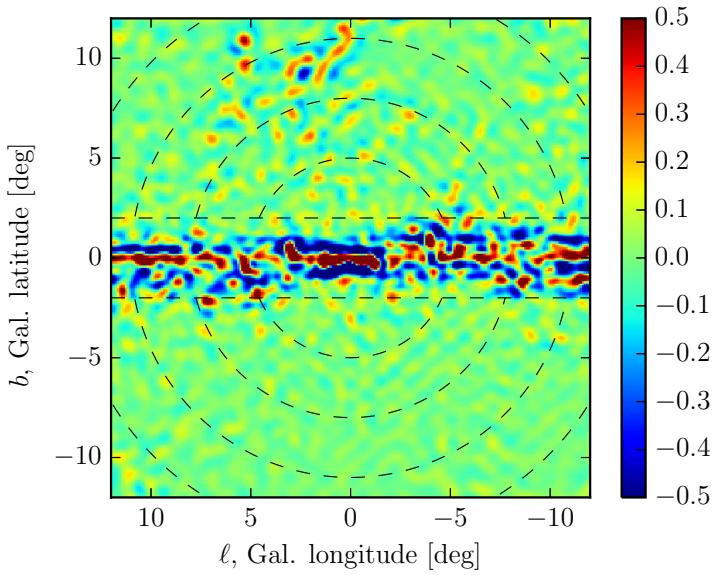

FIG. S-8. Similar to Fig. 1 in the main text (note the different color scale), but showing the transform of the diffuse BG model only, without Poisson noise being applied. Outside of the Galactic disk, $|b| > 2^\circ$, which we exclude from our analysis, the significance of wavelet peaks remains below 0.5. The variance is below 0.1, which shows that even 1σ peaks in the wavelet transform are unlikely to be strongly affected by the Galactic diffuse emission.

sociated (and sub-threshold) sources are likely MSPs, whereas unassociated sources in other parts of the disk have a larger fraction of young pulsars. The latter point is further supported by the fact that similar structures can be found in the longitudinal distribution of identified pulsars.

In summary, we expect that our wavelet signal is dominated by whatever source class is responsible for most of the unassociated sources towards the inner Galaxy. Very likely, these are millisecond and young pulsars, with a somewhat higher MSP/young pulsar ratio than in the rest of the disk. Since these sources appear in general both in the Galactic disk as well as in the bulge, it is important to study whether the excess/suppression of wavelet peaks in the inner Galaxy points to a disk population, a bulge population, or to a combination of both. This will be discussed in the section G below.

F. Possible caveats concerning the Galactic diffuse emission

In our Monte Carlo studies, we use the standard *Fermi* diffuse model for pass 8 data analysis. The wavelet transform of this model, *without applying Poisson noise*, but using the same exposure as in our main analysis, is shown in Fig. S-8. Outside of the masked Galactic disk at $|b| > 2^\circ$, we do not find any excesses with a significance larger than about 0.5σ. The main effect of such variations would be to offset the significance of random statistical fluctuations and sub-threshold point sources towards higher or lower values. This would not significantly affect peaks with a large SNR. However, it can potentially be important for low-significance peaks, because the collective shift of a large number of peaks, even by a small amount, could become statistically relevant. But since the variance of the SNR values shown in Fig. S-8 is below 0.1, we do not expect that the details of the modeling of diffuse emission when doing MCs is going to affect our results.

The *Fermi* diffuse models might not actually contain all relevant small-scale gas structures, and the effect of these missing structures on our results is not straightforward to estimate without a detailed analysis and modeling of the power-spectrum of gas at small scales. It is hence rather important that our non-detection of strong wavelet signals along the Galactic disk in Fig. S-1 largely excludes that mismodeling of *local* gas is the cause for the detected signal towards the inner Galaxy, since it would affect other parts of the disk as well. This is in particular true since there is relatively little molecular gas in our main ROI, compared to the control regions [7]. Thus, gas-related effects should be larger in the control regions than in the main ROI.

If one insists on a gas-related interpretation, our results hence suggest that the wavelet signals are caused by

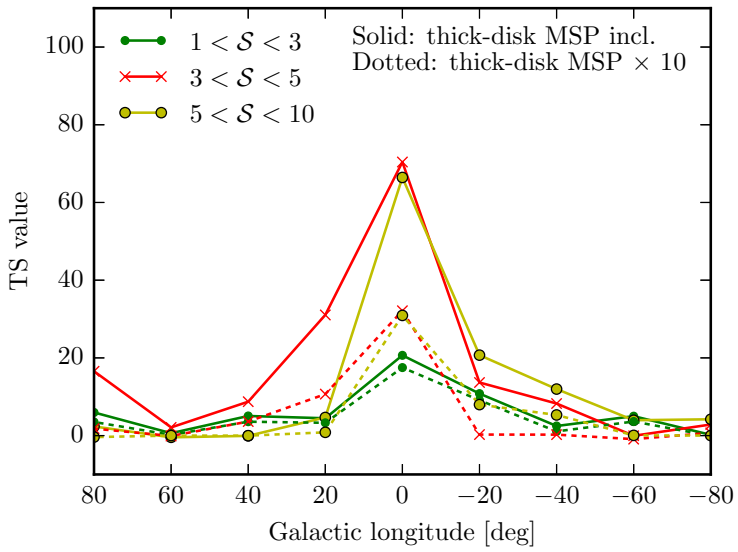

FIG. S-9. Similar to Fig. S-1, but including a thick-disk MSP population calibrated to local bright high-latitude MSPs as additional background. Only for illustration, we also show the effect of a 10× more dense thick-disk population (which is in contradiction with local observations). Note that we unmask 3FGL as described in the main analysis when deriving the wavelet peaks.

unmodeled gas in the Galactic bulge, at a height of 0.3–1.5 kpc. If we assume a cosmic-ray density in the bulge similar to the local one, the differential γ-ray emissivity at 1 GeV is around 3×10^{-26} s^{-1}GeV^{-1} per hydrogen atom [8]. This implies that dense gas clouds with masses around $3 \times 10^5\,\mathrm{M}_\odot$ would be at 1 GeV roughly as bright as MSPs with a luminosity of $L = 7 \times 10^{34}\,\mathrm{erg\,s^{-1}}$.[1] Interestingly, giant molecular clouds are known objects of that mass, and they can be dense enough to appear at GC distance point-like for *Fermi*. However, the scale height of known giant molecular clouds is at the level of a few 10 pc (they usually intersect with the Galactic disk) instead of the required ~ 1 kpc [9]. Furthermore, clouds of that size should give rise to CO emission in the range $\mathcal{O}$(10–100) K km s^{-1}, which is not seen in current observations [7]. If observed, such CO emission should be distributed north/south symmetric, as our wavelet peaks are too.

If one could show that a large number of such giant molecular clouds (or other structures with similar mass and density) can form and be transported to kpc heights in the Galactic bulge, while hiding from all observations, the interpretation of the identified wavelet peaks in terms of unmodeled gas would remain a possibility. However, as of now, and for all of the above reasons, we regard gas-related interpretations of our results as rather unlikely and speculative.

G. Potential impact of thick-disk population

As argued above, the most relevant Galactic background in our ROI are expected to be pulsars, and in particular the MSP thick-disk population that reaches up to high latitudes. We will now show that a thick-disk population of MSPs (or other sources with a similar luminosity function) cannot be responsible for the observed signal.

In most cases, the thick-disk population of MSPs is modeled as a cylindrically symmetric exponential distribution, with a scale height in the range 0.5–1 kpc and a scale radius of a few kpc, which is only poorly constrained by data (see *e.g.* Ref. [10]). We will adopt here a distribution with a scale height of 1 kpc and a scale radius of 5 kpc, which was previously used to argue against the MSP-origin of the *Fermi* GeV excess [11]. The distribution reads $n \propto \exp\left(-R/R_\mathrm{s}\right) \exp\left(-\left|z\right|/z_\mathrm{s}\right)$, with $R_\mathrm{s} = 5\,\mathrm{kpc}$ and $z_\mathrm{s} = 1\,\mathrm{kpc}$. We will address below how the results change when other parametrizations are adopted.

[1] We note for reference that for such a MSP, placed at GC distance, we would have seen around 270 photons in our energy range. From this and Tab. I one can estimate that ~ 100 photons correspond to a wavelet signal with a significance of $\mathcal{S} \sim 2$.

As γ-ray luminosity function, we adopt an inverse power-law with $L_{\rm min} = 10^{31}\,{\rm erg\,s^{-1}}$, $L_{\rm max} = 7\times10^{34}\,{\rm erg\,s^{-1}}$ and index $\alpha = 1.5$. We fix the overall normalization of the disk source density such that the number of bright MSPs at high latitudes, $|b| > 15^\circ$, is consistent with the number of such MSPs listed in the 3FGL. As flux threshold for bright MSPs we adopt a flux that corresponds to a γ-ray luminosity of $10^{34}\,{\rm erg\,s^{-1}}$ at 3 kpc distance ($9.2\times10^{-12}\,{\rm erg\,s^{-1}cm^{-2}}$ in our energy range). We find 31 MSPs above that threshold flux and note that since the number of unassociated high-latitude bright nonvariable sources with a curved enough spectrum is small, this number cannot increase by more than 50% when more unassociated sources are identified as MSPs) [12]. For the present scenario, we find that the total number of thick-disk sources with γ-ray luminosity above $10^{31}\,{\rm erg\,s^{-1}}$ is ~ 30000.

Within 2 kpc of the Galactic center, this thick-disk population predicts around 1300 MSPs, which is more than an order of magnitude below the number that we find in the best-fit scenario for the bulge population (around 35000 MSPs above $10^{31}\,{\rm erg\,s^{-1}}$). This implies, as already argued in Ref. [11], that a thick-disk population with the adopted geometry cannot be responsible for the *Fermi* GeV excess. However, it also trivially implies that the number of wavelet peaks caused by thick-disk sources in the inner 2 kpc is about an order of magnitude below what is predicted by our best-fit bulge population, and hence an order of magnitude below what is actually observed. This still leaves the possibility that thick-disk MSPs on the line-of-sight towards the inner Galaxy, outside of the inner ~ 2 kpc, could affect our results. We will discuss this next.

Within our ROI, the thick-disk population predicts 3.3 sources outside of the inner 2 kpc with a flux in the range $(4.6\text{–}7.7)\times10^{-12}\,{\rm erg\,s^{-1}cm^{-2}}$ (this corresponds roughly to $(4\text{–}7)\times10^{34}\,{\rm erg\,s^{-1}}$ when the sources are put at 8.5 kpc distance). These sources could reasonably contribute to wavelet peaks in the $3 < \mathcal{S} < 5$ range. The actually observed number of peaks in that range above the null hypothesis is about 35. It is hence clear that foreground sources from the above thick-disk population cannot cause the observed signal. One might think of two ways around.

First, one could reduce the scale radius of the thick-disk population such that the number of sources in the inner 2 kpc increases by a factor around ten (scale radii around 1–2 kpc could do the job). This would give rise to a wavelet signal similar to what is observed. However, such a population would also predict a significant diffuse γ-ray emission similar to the level of the *Fermi* GeV excess, just with a morphology that is incompatible with the observations. A population with a scale radius of 1–2 kpc would indeed commonly be referred to as bulge population. Such a population would be very similar to the bulge population that we put forward in the main part of the paper as explanation for the *Fermi* GeV excess, with the main difference being that our population fits better the excess morphology.

Second, one could increase the number of MSPs in a ring-like region around the Galactic bulge, excluding the inner 2 kpc, such that these additional ring-like distributed sources will enhance the number of foreground sources without affecting the number of sources in the Galactic bulge. In this case, however, the wavelet signal should clearly be more extended along the Galactic disk than what is shown in Fig. S-1, since such a ring would not be centrally peaked and extend to longitudes of at least $\sim 25^\circ$. For illustration, we here quote the relative number of wavelet peaks one expects in the control regions along the disk and the main ROI produces by such a ring (1 kpc scale height, 5 kpc scale radius, the inner 2 kpc radius excluded): $\Delta\ell = \{\pm80, \pm60, \pm40, \pm20, 0\}$ and $N_{\rm peaks} \propto \{1.7, 2.4, 3.5, 4.9, 3.6\}$. Moreover, in order to avoid a conflict with the above calibration with bright high-latitude sources, the ring should be further constrained to lie within $\lesssim 5$ kpc, which however would still leave a too flat central distribution of wavelet peaks.

Finally, we show in Fig. S-9 how the TS values are affected if the thick-disk population (or a $10\times$ denser population) is added as an additional background component. For simplicity, we assume that the thick-disk population causes deviations of the expectation values μ_{ij} in Eq. (3) from the null hypothesis that are proportional to the deviations caused by the best-fit bulge population. We adjust the normalization of these deviations such that the number of additionally predicted $3 < \mathcal{S} < 5$ peaks in the main ROI is 3.3 (as motivated by the above discussion). We then add these thick-disk-induced deviations from the null hypothesis as negative and positive contributions to the model predictions in Eq. (3), and repeat the CSP fit to inner Galaxy data. We repeat this procedure in all of the control ROIs used in Fig. S-1, reweighing the thick-disk contribution properly at different Galactic longitudes. From Fig. S-9 it is clear that only a thick disk ten times denser than what is actually observed at higher latitudes could significantly affect, although not completely remove, the excess of wavelet peaks in the inner Galaxy.

H. Further discussions

In order to test whether the spatial distribution of wavelet peaks in our analysis is indeed compatible with a spherically symmetric distribution, we re-binned the wavelet peaks into a north/south region, defined by $12^\circ > |b| >$

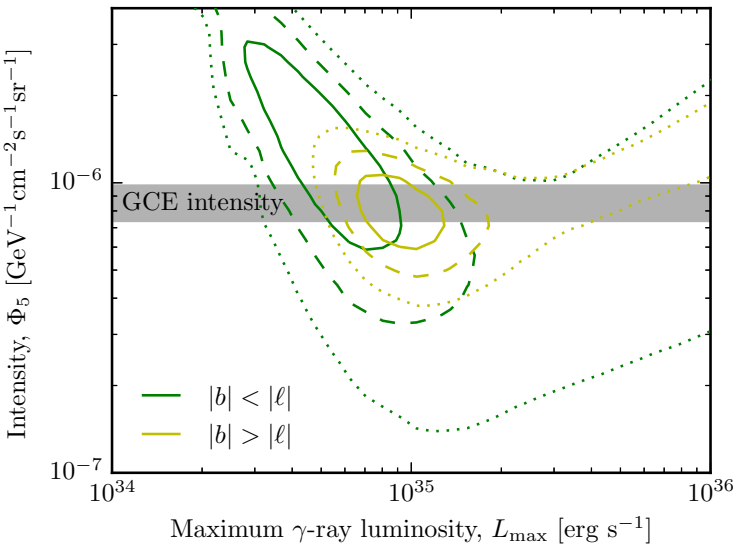

FIG. S-10. Similar to Fig. 3 in the main text, but derived in redefined regions within our main ROI that are useful to check for the sphericity of the signal (we still mask $|b| < 2^\circ$). We find best-fit parameters for $L_{\rm max}$ and Φ_5 in the north/south and east/west regions that are consistent within one sigma.

$\max(|\ell|, 2^\circ)$, and an east/west region, defined by $12^\circ > |\ell| > |b| > 2^\circ$. For each of the two regions, we derive the best-fit values for $L_{\rm max}$ and Φ_5. The results are shown in Fig. S-10. We find that the inferred parameters are consistent within one sigma, with a slightly stronger signal in the north/south region. This indicates that the excess of wavelet peaks, if interpreted in terms of a bulge source population, is consistent with a spherical distribution of these sources.

Given that unresolved sources only add positively to the Galactic diffuse emission, whereas a mismodeling of the gas could cause both positive and negative variations, it is tempting to think that a detection of negative wavelet peaks would disfavour an interpretation in terms of unresolved point sources. In fact, we do find a suppression of $-2 < \mathcal{S} < -1$ peaks, and an enhancement of $-4 < \mathcal{S} < -3$ peaks in the inner ROI when searching for negative instead of positive peaks. But unfortunately, this cannot easily be used to discriminate diffuse modeling artefacts (which, as we discussed above, are anyway unlikely, as they should show up in the entire disk) from sub-threshold point sources.

Maybe somewhat un-intuitively, negative wavelet peaks can indeed be generated by a large number of weak, positive point sources. This happens in the tails of our simulated sources, where the wavelet transform becomes negative (this effect is visible as rings around bright sources in Fig. 1). We estimated the expected number of *negative* wavelet peaks for the best-fit scenario in Fig. 3 by Monte Carlo simulations, and find results that are completely consistent with the observed number of negative peaks. However, given that the number of positive and negative wavelet peaks are correlated (they are caused by the same sources), one cannot easily use observations of negative wavelet peaks to further constrain the model parameters. This, and the fact that an appropriate masking of 3FGL sources (including also the ring around each source) reduces significantly the effective size of the ROI, make an efficient use of negative peaks in our analysis difficult. However, it is re-ensuring that both the observed negative and positive wavelet peaks are consistent with the respective predicted number of negative and positive wavelet peaks for the same sub-threshold point source population.

Finally, we briefly comment on the recent analysis of the Galactic center data by the *Fermi*-LAT collaboration [13] and compare their use of wavelets to ours. Ref. [13] uses wavelets to find seeds for the identification of point sources (also see Ref. [14] for details about the adopted method), followed by standard maximum-likelihood fits for further source identification. This can be potentially affected by interstellar emission modelling. We instead study the statistics of local-maxima in the wavelet-transformed sky map, which is largely background-model independent (although small scale fluctuations could in principle be relevant, as discussed above). We find good correspondence between our wavelet peaks and the 3FGL catalogue (see Fig. 1), which supports the validity of our approach. However, we also find that this agreement and the quality of the wavelet analysis in general critically depends on the adopted wavelet type and size. All these points make it difficult to directly compare our results with those of Ref. [13]. However, we note that the Galactic disk, where Ref. [13] finds that their identified sources most strongly trace the

edges of the interstellar emission and thus might constitute false positives due to gas fluctuations (see their Fig. 8), is masked in our analysis.

* r.t.bartels@uva.nl
† s.krishnamurthy@uva.nl
‡ c.weniger@uva.nl

[1] F. Calore, I. Cholis, and C. Weniger, JCAP **1503**, 038 (2015), arXiv:1409.0042 [astro-ph.CO].
[2] A. W. Strong, Astrophys.Space Sci. **309**, 35 (2007), arXiv:astro-ph/0609359 [astro-ph].
[3] C. Venter, T. Johnson, A. Harding, and J. Grove, (2014), arXiv:1411.0559 [astro-ph.HE].
[4] J. Petrovi, P. D. Serpico, and G. Zaharijas, JCAP **1502**, 023 (2015), arXiv:1411.2980 [astro-ph.HE].
[5] I. Cholis, D. Hooper, and T. Linden, (2014), arXiv:1407.5583 [astro-ph.HE].
[6] T. D. Brandt and B. Kocsis, (2015), arXiv:1507.05616 [astro-ph.HE].
[7] T. Dame, D. Hartmann, and P. Thaddeus, Astrophys.J. **547**, 792 (2001), arXiv:astro-ph/0009217 [astro-ph].
[8] J.-M. Casandjian, Astrophys. J. **806**, 240 (2015), arXiv:1506.00047 [astro-ph.HE].
[9] A. A. Stark and Y.-G. Lee, Astrophys. J. **619**, L159 (2005), arXiv:astro-ph/0403631 [astro-ph].
[10] T. Gregoire and J. Knödlseder, (2013), arXiv:1305.1584 [astro-ph.GA].
[11] I. Cholis, D. Hooper, and T. Linden, (2014), arXiv:1407.5625 [astro-ph.HE].
[12] The Fermi-LAT Collaboration, ArXiv e-prints (2015), arXiv:1501.02003 [astro-ph.HE].
[13] M. Ajello *et al.* (Fermi-LAT), (2015), arXiv:1511.02938 [astro-ph.HE].
[14] F. Damiani, A. Maggio, G. Micela, and S. Sciortino, The Astrophysical Journal **483**, 350 (1997).